SAND2007-5228C

COMPUTER SIMULATIONS OF THE MAGNETICALLY INSULATED TRANSMISSION LINES AND POST-HOLE CONVOLUTE OF ZR*

T. D. Pointon[ξ], W. L. Langston, and M. E. Savage
Sandia National Laboratories, PO Box 5800, Mail Stop 1152
Albuquerque, NM 87185 USA

Abstract

An important consideration for the success of the ZR project, refurbishing the Z accelerator at Sandia National Laboratories, is limiting current loss in the vacuum section, ideally to no worse than the 5 – 10% seen on Z. The primary source for this loss is electrons flowing into the post-hole convolute from the four magnetically insulated transmission lines (MITLs). The MITLs on ZR have larger gaps to reduce the electron flow to values comparable to Z when operating at ~40% higher voltage and ~30% higher current.

Electron flow in the vacuum section is analyzed with electromagnetic, particle-in-cell simulations, using two complementary simulation setups. First, the exact MITL profiles are modeled with high-resolution 2-D simulations out to large radius (typically r = 60 cm), providing accurate values for the electron flow into the convolute. Second, the convolute is modeled in 3-D, but with MITLs extending out only to r ~ 30 cm. The 3-D MITL geometry is modified to provide the same electron flow into the convolute as the 2-D simulations. The 3-D simulations have detailed diagnostics for current loss and surface deposition heating in the convolute.

I. INTRODUCTION

The vacuum section of ZR[1] is topologically identical to the original Z vacuum section,[2] shown in Fig. 1. Power is conducted radially inward from the vacuum insulator stack at r ~ 1.6 m towards the load with four magnetically insulated transmission lines (MITLs), denoted A – D from top to bottom, coupled in parallel with a double post-hole convolute. There are 12 posts, at r = 7.62 cm, connecting the three anodes between holes in the two cathodes. On ZR, the load height has been raised 16 inches relative to the insulator stack, to provide better diagnostic access, which increases the MITL slope. Furthermore, the MITL gaps have opened up by 20% for r > ~18 cm to reduce the electron flow. Both changes increase the MITL inductance, particularly on the lower levels, as shown in Table 1.

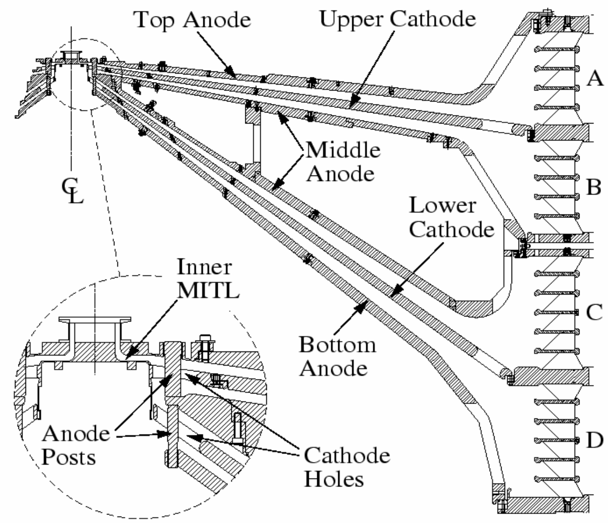

Figure 1. Vacuum section of the Z accelerator, with inset showing the convolute. Power flows to the left from the insulator stack at the far right at r ~ 1.6 m.

Table 1. Cathode MITL angle relative to horizontal, and MITL inductance (11 < r < 125 cm) for Z and ZR.

Level	Angle (degrees)		L (nH)	
	Z	ZR	Z	ZR
A	8.1	24.9	9.01	11.57
B	9.1	26.0	9.30	12.42
C	35.9	48.9	13.54	19.63
D	36.7	49.7	14.18	21.99

As the power pulse propagates radially inward, the threshold for electron emission from the MITL cathodes is rapidly exceeded. Except for a brief period early in the pulse (much longer on D-level), the magnetic field from the conductor current inhibits electron loss to the MITL anodes, and the electrons **E**×**B** drift into the convolute. In the convolute, there are "magnetic nulls", paths

---

* Sandia is a multiprogram laboratory operated by Sandia Corporation, a Lockheed Martin company, for the United States Department of Energy's National Nuclear Security Administration under contract DE-AC04-94-AL85000.

ξ email: tdpoint@sandia.gov

connecting the anode and cathode where $|\mathbf{B}| = 0$, shown in Fig. 2. There is a null connecting each post with the corresponding cathode in the plane cutting through the center of a post, and a null connecting the middle anode to the upper cathode midway between a pair of posts. In addition, there is an azimuthally-symmetric null connecting the central cathode to the bottom anode. In these regions, magnetic insulation breaks down. Intense localized electron deposition heating of the anode can occur in these regions.

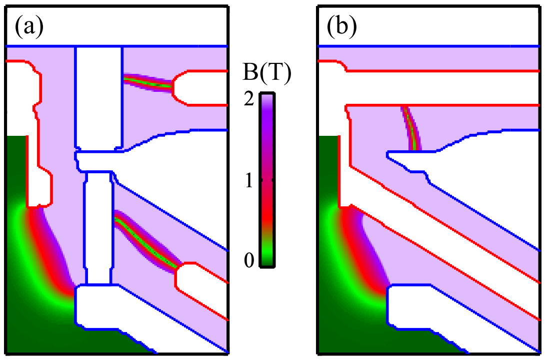

Figure 2. Magnetic nulls in the Z convolute, shown with contours of $|\mathbf{B}|$ for (a) a plane through the center of the post, and (b) a plane midway between the posts. The color scale highlights the magnetic nulls; the peak value in the convolute is B ~ 50 T.

Results from earlier 3-D simulations showed that vacuum electron losses in the convolute can account for the current loss between the MITL and the load on Z early in the pulse.[3] However, late in the pulse, the current loss in experiments becomes progressively higher than the simulations. Another mechanism, presumably associated with dense electrode plasmas, is responsible for most of the current loss late in time.

In this paper, we describe results of new 2-D and 3-D simulations of the Z and ZR vacuum sections with the particle-in-cell (PIC) code QUICKSILVER.[4] Results from earlier 3-D simulations of the Z convolute,[3,5] show that the MITLs can be simulated in 2-D. First, even slightly upstream of the convolute, the boundary and electron flow currents in the MITLs are essentially azimuthally symmetric. Second, until the load stagnates, there are no electrons flowing back into the MITLs from the convolute. The electron flow through the "convolute"/MITL boundary at r ~ 11 cm in the 2-D simulations closely approximates the actual flow into the convolute. The 2-D MITL results presented in Section II improve on earlier work[6] by modeling all four levels simultaneously with separate 2-D PIC simulation regions. In Section III, we present results of new 3-D convolute simulations, with accurate electron flow into the convolute. Detailed diagnostics show where the electrons are lost, and compute the electron energy deposition into the anode. In Section IV, we summarize the results and discuss future plans.

II. 2-D MITL SIMULATIONS

A. Introduction

For an infinitely long MITL with uniform vacuum impedance Z_0, the line is insulated at a given voltage when the current exceeds a threshold value. For a fixed resistive load in equilibrium, the electron flow current I_e, anode boundary current I_a, and cathode boundary current I_c satisy $I_a = I_c + I_e$. The voltage and currents are related to a good approximation by [7]

$$V = Z_0 (I_a^2 - I_c^2)^{1/2} - \frac{mc^2}{2e}\left(\frac{I_a^2}{I_c^2} - 1\right) \cdot \qquad (1)$$

For a strongly undermatched load, $Z_L << Z_0$, the electron flow is much smaller than the boundary currents, and is confined to a thin sheath at the cathode. For a radial transmission line, the vacuum impedance varies with radius, $Z_0 = 60d/r$, where d(r) is the gap. Applying Eq. 1 locally in r, in the limit $Z_L << Z_0$, where $I_a \sim I_c = I$, the flow current and sheath thickness, g, are approximately

$$I_e(r) \cong \frac{Z_L^2}{2Z_0^2} I \propto \frac{V^2}{I}\frac{r^2}{d^2}, \text{ and} \qquad (2)$$

$$g(r) \cong \frac{mV}{eB^2 d} \propto \frac{V}{I^2}\frac{r^2}{d} \cdot \qquad (3)$$

The impedance profile for the Z A-level MITL is shown in Fig. 3a. The gap is constant, d = 1 cm, for r < 20 cm, resulting in a rapidly varying Z_0 in this region. The other MITLs have a similar profile. On ZR, the constant 1 cm gap section is only for r < 13.6 cm, opening up to 1.2 cm at r ~ 18 cm. Simulations show that when the MITL is strongly insulated, the electron flow is unstable at small radius, where $|dZ_0/dr|$ is relatively large. This is illustrated in Fig. 3b, from a run with constant $Z_L = 0.575\ \Omega$. The electron flow current profile agrees very well with Eq. 2 for r > ~30 cm, where the electron sheath is essentially laminar. However, the vortices enhance the flow current into the convolute by a factor of 3 – 4. Eq. 3 predicts very thin electron sheaths at peak current, as shown in Fig. 3b.

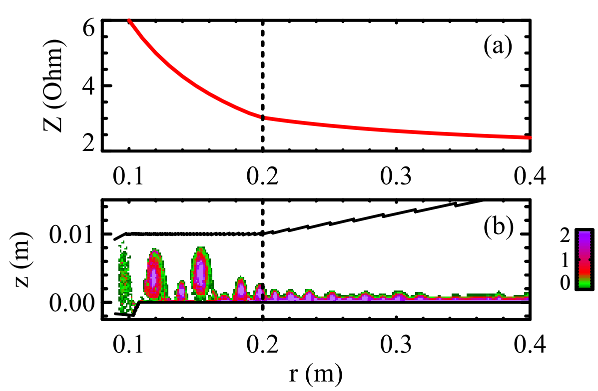

Figure 3. (a) Vacuum impedance profile for the Z A-level MITL, and (b) contours of electron density from a 2-D simulation of this MITL.

B. Four-Level, Time-Accurate Simulation Setup

To model Z and ZR with a time-accurate power pulse and Z-pinch load, we use a simulation setup with four separate 2-D PIC regions, one for each MITL, coupled together with 1-D transmission lines. Each PIC region accurately simulates the MITL geometry from the convolute/MITL boundary at r = 11 cm out to large radius. The outer radius needs to be well upstream of where the electron vortices shown in Fig. 3b form. We typically use r = 60 cm. The simulations are done in spherical coordinates to avoid "stairstepping" the cathode. Each MITL is independently shifted in z so that the cathode lies on a θ = *const* surface in its own 2-D region.

The outer radial boundary of each region connects to 1-D transmission lines modeling the upstream geometry, out to the constant impedance lines in the water section. Similarly, the inner radial boundaries are connected to a 1-D transmission line model of the convolute and load. The model also includes additional current loss in the convolute. Circuit simulations of Z usually use a "Z-flow" loss term, relating the voltage, and upstream and downstream currents by

$$V = Z_L (I_u^2 - I_d^2)^{1/2}, \quad (4)$$

where Z_L is typically a constant 0.25 Ω. Eq. 4 has a physical basis for describing electron loss at a single magnetic null.[8]

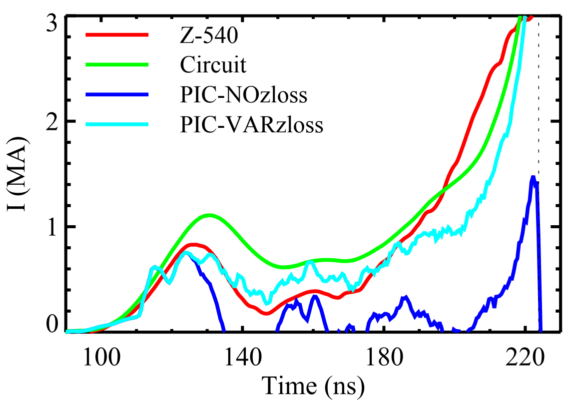

Figure 4. Convolute loss current from data for Z shot 540, compared with a circuit simulation using a constant 0.25 Ω, and full, four-level 2-D PIC simulations, both with and without the additional $Z_L(t)$ term. Peak current is at t = 200 ns, and the pinch implodes at t = 224 ns.

The 2-D PIC simulations have vacuum electron losses, both directly to the anode, and flowing out through the inner boundaries (reducing the current coupled to the inner 1-D transmission lines). Fig. 4 compares the current loss, the difference between the MITL and load currents, for Z shot 540 and simulations. The vacuum electron loss in the PIC simulation matches the initial loss on Z quite well. To improve the agreement later in the pulse, we add an additional *time-dependent* loss in the convolute. Since loss based on Eq. 4 is already implemented in the code, we use this form, smoothly transitioning from a high initial value Z_{Li} to a final value Z_{Lf} according to

$$Z_L(t) = Z_{Lf} + \tfrac{1}{2}(Z_{Li} - Z_{Lf})(1 + \tanh[\beta(t_0 - t)]). \quad (5)$$

Results for a PIC simulation using this model with parameters Z_{Li} = 5 Ω, Z_{Lf} = 0.32 Ω, t_0 = 125 ns, and β^{-1} = 3 ns, are also shown in Fig. 4. It fits the loss better than the circuit simulation for t < 190 ns. However, both simulations underestimate the loss for t > 200 ns. A better fit to the data clearly requires a loss impedance that is continuously decreasing late in the pulse.

C. Electron Flow Current into the Convolute

Since the variable $Z_L(t)$ term gives a better fit to the peak load current and convolute loss, we use it in the simulations to compare the electron flow into the convolute for Z and ZR. Without experimental data for ZR, we use the same $Z_L(t)$ as the Z simulations, except that the transition time is modified. For the Z simulation, we integrate the flow current into the convolute from t = 0 to t = t_0, giving a net charge Q_{0Z}. We then set t_0 for ZR as the time at which the flow current integral equals Q_{0Z}.

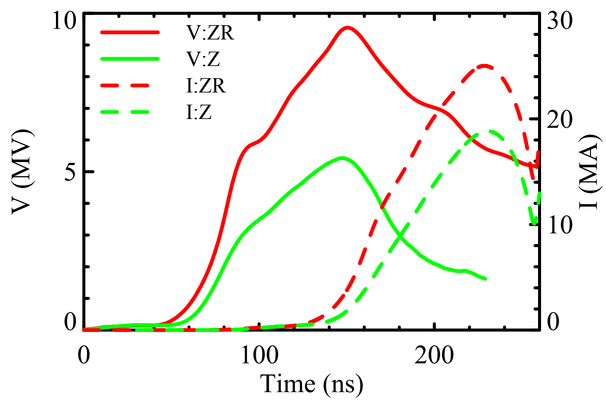

Figure 5. Comparison of the open-circuit voltage used to drive the Z and ZR simulations, and the load current. The Z load current is time-shifted to have the same pinch time.

The open-circuit voltage waveforms used to drive the simulations is shown in Fig. 5. The Z waveform comes from shot data, the ZR one from the Z20 facility used to prototype a single ZR pulse-forming line.[9] Also shown is the load current from circuit simulations with constant Z_L = 0.25 Ω. The peak load current is 25.0 MA for ZR, and 18.8 MA for Z. The Z-pinch load for the simulations uses the "Z shot 51" parameters: 2 cm tall, 2 cm diameter, with an initial gap between the wire array and return current can of 5 mm. The wire array mass is 4.315 mg for Z, and 9.2 mg for ZR. The implosion time for ZR is about 10 ns longer. When comparing results between ZR and Z, we always time-shift the Z data to have the same pinch time.

Results for the electron flow into the convolute are shown in Fig. 6. The flow current has been time-integrated to give the charge flowing into the convolute. The flow is considerably lower for the upper two levels. Even though the flow is higher on ZR on these levels, this is only a small increase in the net flow into the convolute. On C-level, the flow is lower on ZR than on Z. However, the D-level flow is 12% higher on ZR. Summed over all four levels, the flow is 4% higher on ZR.

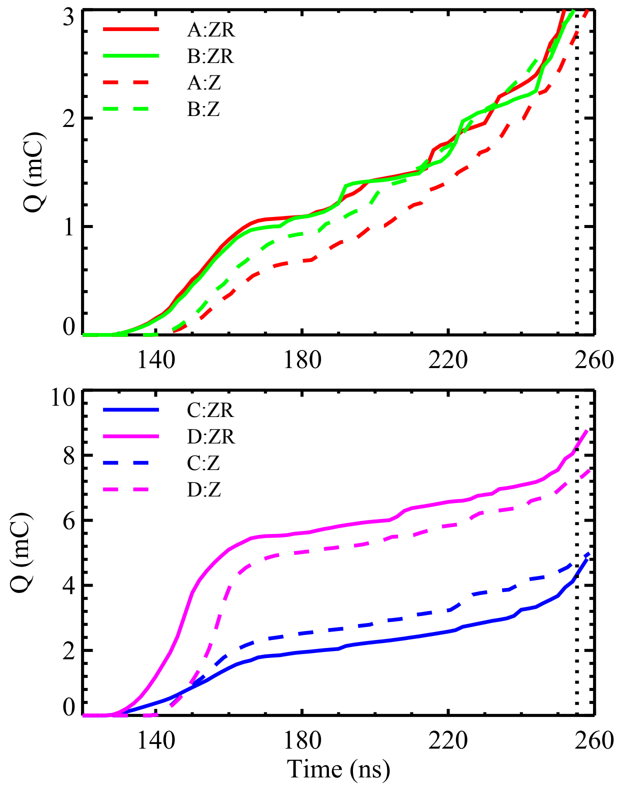

Figure 6. Comparison of the time history of the charge flowing into the convolute for ZR (solid lines) and Z (dashed lines) on all four levels. The Z data is time-shifted to align the pinch time (dotted black line).

III. 3-D CONVOLUTE SIMULATIONS

A. Simulation Setup

The 3-D convolute simulations are done in cylindrical coordinates, modeling a 1/24 pie slice in azimuth. There are 30 azimuthal cells, with the $\phi = 0$ plane at the middle of a post, and the $\phi = \phi_{max} = \pi/12$ plane midway between two posts. The MITLs must necessarily be zoned much more coarsely than the 2-D simulations. We typically use 30 cells across the MITL A-K gaps (compared to 10 for earlier convolute simulations,[3,5] and 100 or more for the 2-D simulations). We avoid stairsteps at the MITL cathodes by using a slanted surface model.[10] This model is used for all conical surfaces in the convolute, both the cathodes and the anodes. However, the posts and cathode holes must still use conventional stairstepped conductors.

The geometry used for the ZR convolute simulations is shown in Fig. 7. The computational domain is the union of the simulation "blocks", which all use the same azimuthal grid. However, Δr and Δz can be independently varied in disconnected blocks. Thus, using these blocks not only reduces the cell count, but allows the MITL blocks to use r-z grids fitted exactly to their cathode slope. The Z simulations use a similar geometry, except that the A and B MITLs are modeled with purely radial lines, as done in earlier simulations.

Just upstream of the convolute, the MITLs are smoothly bent into purely radial lines. Originally, we extended the slanted surfaces out to r = 30 cm, but the slanted surface model has problems when the electron sheath thickness is comparable to the cell size. For a conformal emission surface, even when the sheath thickness is much smaller than the normal cell size we usually get roughly the correct electron flow. However, at slanted surfaces, the electrons are confined to a very thin layer just above the cathode, and the flow current is greatly reduced. This appears to be an intrinsic limitation of the slanted surface model (although it works well for other problems). Thus, we modify the MITL geometry to provide a conformal emission surface upstream of the slanted MITL section.

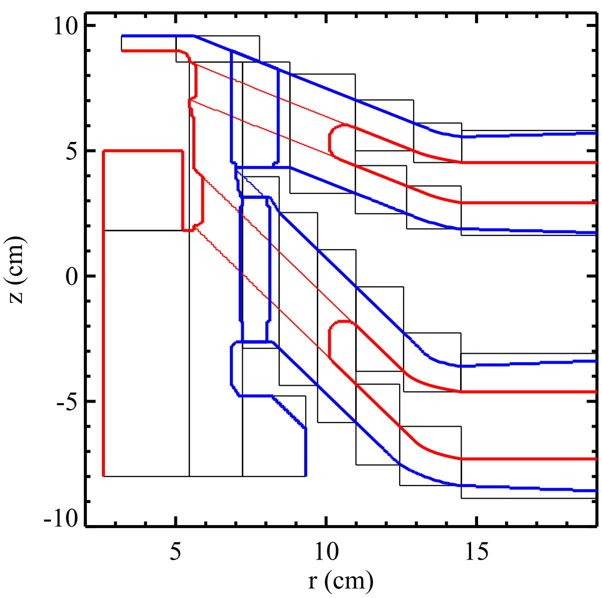

Figure 7. ZR convolute simulation geometry. The simulation "blocks" are shown in black, the anode in blue, and the cathode in red. The thin conductor lines are for $\phi = \phi_{max}$. The MITLs extend out to r = 33 cm on the upper levels, and r = 36 cm on the lower levels.

B. Electron Flow Current into the Convolute

The modified geometry of the MITLs means that we cannot compute the electron flow into the convolute from first principles. Instead, we use two adjustable parameters to match the flow current to the 2-D simulations. The first parameter is the outer radius at which the A-K gap follows the actual MITL gap. Beyond this radius, the gap is constant. The second parameter is the maximum radius for electron emission. We use 2-D r-z simulations to more rapidly iterate these parameters. Results from a 3-D convolute simulation with the latest iteration of the MITL geometry are shown in Fig. 8. This simulation uses the same open-circuit voltage waveform and Z-pinch load as in Section II. Since the 3-D convolute simulation only has vacuum electron loss, the 2-D data in Fig. 8 differs from Fig. 6 because we are not using any additional convolute current loss. The agreement is excellent on the upper two levels. Agreement is not quite as good on the lower levels; the 3-D flow is higher on C-level, and lower on D-level. Currently, our geometry-building tools are limited to using the same radial parameters for these two levels. In future, we will modify these tools so that the C and D MITLs can be constructed independently.

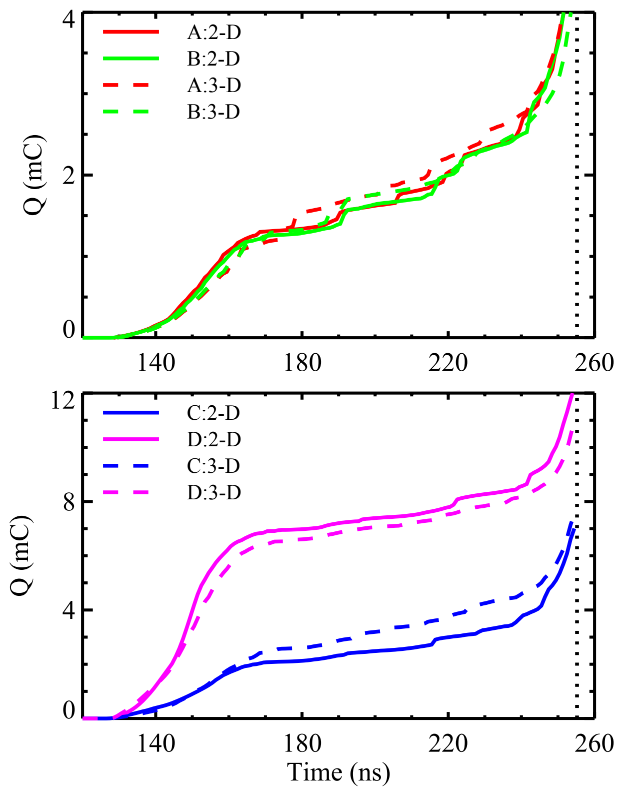

Figure 8. Comparison of the time history of the charge flowing into the ZR convolute for 2-D (solid lines) and 3-D (dashed lines) on all four levels.

The comparison of the flow current into the convolute for 3-D Z and ZR simulations is very similar to Fig. 6. The flow on ZR is slightly higher on A and B levels, slightly lower on C-level, and 14% higher on D-level. The net flow is 5% higher on ZR.

C. Electron Deposition Heating in the Convolute

We compute electron deposition heating using the same procedure as Ref. 11. Using ITS,[12] we construct a 2-D table of the specific energy deposition $Q(E_i,\mu_j)$, for a set of discrete incident energies E_i, and angles $\mu_j = \cos(\theta_j)$. When an electron passes through any anode conductor face, including slanted surfaces, we interpolate Q from the table, and increment the temperature at the four corners of the face using bilinear weighting from the particle position.

Spatial snapshots of the anode temperature in the convolute and inner MITL are saved at 2 ns intervals. In a post-processing step, we construct time histories of the peak temperature for selected regions. Some results of this analysis are presented in Fig. 9. The time-shifting of the Z data is particularly relevant here, since the most important consideration is how long before the pinch implosion the temperature rises above a threshold value. We have plotted the line T = 400 ^{o}C on these figures, a widely accepted threshold value for the onset of plasma formation on the surface.[13]

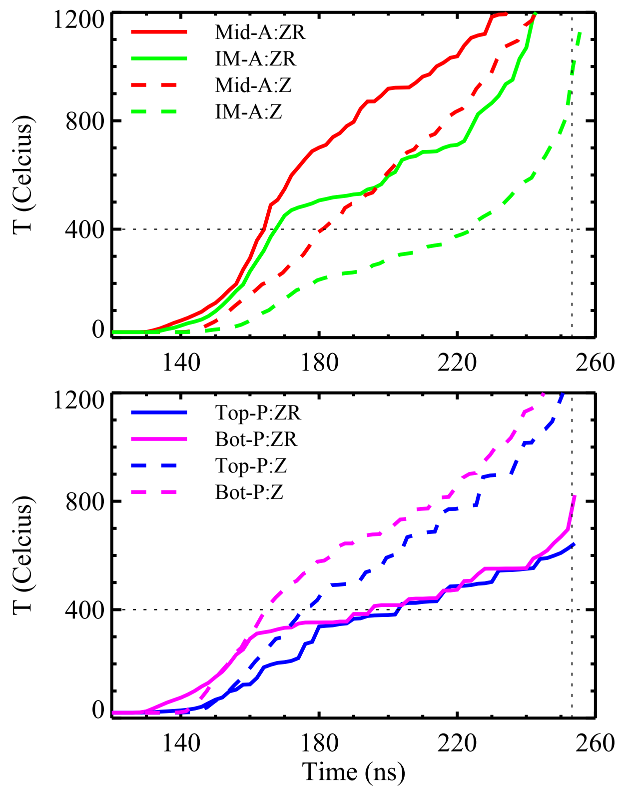

Figure 9. Peak anode temperature as a function of time for anode regions of the convolute for ZR (solid lines) and Z (dotted lines): upper surface of the middle anode, the inner MITL, and the top and bottom posts. The Z-data is time shifted to align the pinch time.

For both ZR and Z, the most rapidly heated magnetic null region is the upper surface of the middle anode (see Fig. 2b). On ZR, the heating of the inner MITL is substantially faster. However, the heating of the posts is significantly lower. For some reason, a greater fraction of the MITL electrons are missing the posts, and going up into the inner MITL, where the A-K gap is only 6 mm. If this enhances gap closure of the inner MITL, the gap may have to be increased.

IV. SUMMARY AND FUTURE PLANS

At this point, we have time-accurate simulation models of vacuum electron flow in both the MITLs and the convolute. The 2-D MITL simulations provide accurate values for the electron flow into the convolute. The 3-D convolute simulations show where these electrons are lost, and how rapidly the anode surfaces are heated.

Our near-term plans are to modify these models to study the effect of adding debris shields in the ZR MITLs.[14] We are also continuing to analyze the data from simulations already completed. In particular, we want to understand why the distribution of electron loss is different in the Z and ZR convolutes.

Finally, we are enhancing the code to model dense electrode plasmas. We now have an energy-conserving particle pusher that circumvents numerical heating up to the explicit-PIC density limit $\omega_p \Delta t \sim 1$. With the timestep we are currently using, $\Delta t = 0.5$ ps, we can simulate plasma density up to $n = 10^{15}$ cm^{-3}. Work is underway to implement a model for plasma creation at surfaces exceeding a threshold temperature.

V. REFERENCES

[1] E. A. Weinbrecht, D. D. Bloomquist, D. H. McDaniel, *et al.*, "Status of the Z Refurbishment Project (ZR) at Sandia National Laboratories," in Proc. 15th IEEE Int. Pulsed Power Conf., 2005, p. 170.

[2] W. A. Stygar, *et al.*, "Design and Performance of Z Magnetically Insulated Transmission Lines", in Proc. 11th IEEE Int. Pulsed Power Conf., 1997, p. 591.

[3] T. D. Pointon and W. A. Stygar, "3-D PIC Simulations of Electron Flow in the Vacuum Power Flow Section of the Z Accelerator" in Proc. 13th IEEE Int. Pulsed Power Conf., 2001, p. 1696.

[4] J. P. Quintenz, D. B. Seidel, *et al.*, "Simulation codes for light-ion diode modeling," Lasers and Particle Beams, vol. 12, pp. 283-324, 1994

[5] T. D. Pointon, *et al.*, "Particle-in-Cell Simulations of Electron Flow in the Post-Hole Convolute of the Z Accelerator," Phys. Plasmas, vol. 8, pp. 4534-4544, 2001.

[6] T. D. Pointon and M. E. Savage, "2-D PIC Simulations of Electron Flow in the Magnetically Insulated Transmission Lines of Z and ZR", in Proc. 15th IEEE Int. Pulsed Power Conf., 2005, p. 151.

[7] C. W. Mendel, Jr., *et al.*, "Experiments on a current-toggled plasma-opening switch", J. Appl. Phys, vol. 71, pp. 3731-3746, 1992.

[8] C. W. Mendel, Jr., *et al.*, "Losses at Magnetic Nulls in Pulsed-Power Transmission Line Systems", Phys. Plasmas, vol. 13, 043105-1, 2006.

[9] E. Dawson, Jr., *et al.*, "Towards the Autonomous Operation of Z20: a TW Pulsed Power Module", in Proc. 15th IEEE Int. Pulsed Power Conf., 2005, p. 166.

[10] T. D. Pointon, "Slanted Conducting Boundaries and Field Emission of Particles in an Electromagnetic Particle Simulation Code", J. Comput. Phys., vol. 96, pp. 143-162, 1991.

[11] R. A. Vesey, et al., "Electron-anode interactions in particle-in-cell simulations of applied-B ion diodes", Phys. Plasmas, vol. 6, pp. 3369–3387, 1999.

[12] B. C. Franke, R. P. Kensek, T. W. Laub, "ITS Version 5.0: The Integrated TIGER Series of Coupled Electron/Photon Monte Carlo Transport Codes with CAD Geometry," Sandia National Laboratories Technical Report SAND2004-5172, 2005.

[13] M. E. Cuneo, "The Effect of Electrode Contamination, Cleaning and Conditioning on High-Energy Pulsed-Power Device Performance", IEEE Trans. Dielectr. Elect. Insul., vol. 6, pp. 469-485, 1999.

[14] M. E. Savage, *et al.*, "Passive Mitigation of Load Debris in a Magnetically Insulated Transmission Line", in Proc. 15th IEEE Int. Pulsed Power Conf., 2005, p. 398.